JOURNAL OF SOLID STATE CHEMISTRY 106, 357–371 (1993)

Infrared Spectroscopic Study of Sputtered Tungsten Oxide Films

J-L. PAUL AND J-C. LASSÈGUES*

Laboratoire de Spectroscopie Moléculaire et Cristalline, URA CNRS 124, Université de Bordeaux I, 351 Cours de la Libération, 33405 Talence Cedex, France

Received September 21, 1992; in revised form January 27, 1993; accepted February 1, 1993

Recent infrared and Raman spectroscopic studies of various tungsten oxide films concluded either the formation of W=O terminal bonds or the transformation of such bonds into W–OH groups upon proton insertion. The infrared transmission and reflection spectra of bleached and colored sputtered films were reinvestigated in order to resolve the previous contradictory interpretations and for better insight into the mechanism of electrochromism at the molecular level. The new results confirm the first interpretation and allow us to show that H^+ or Li^+ insertion creates shorter (~1.7 Å) and longer (~2 Å) W–O bonds around the W^{5+} centers. These results are in agreement with the concepts of small polaron and of intervalence charge transfer mechanism. They illustrate the local lattice distortion around a W^{5+} site. Ageing of the initial films has also been followed and characterized by H/D *in situ* isotopic exchange.

Introduction

There is general agreement on the basic reaction of electrochromism in WO_3,

$$WO_3 + xM^+ + xe^- \rightleftarrows M_xWO_3 \text{ (dark blue)}, \quad (1)$$

where $M^+ = H^+, Li^+, Na^+$, etc. . . . .

However, the exact mechanism at a molecular level is still not fully understood, especially in the case of the thin amorphous and nonstochiometric films used in applications for smart windows or displays (*1*).

Recent spectroscopic studies even lead to contradictory conclusions. Daniel *et al.* (*2*) investigated sputtered tungsten oxide films by infrared and Raman spectroscopies. Delichère *et al.* (*3*) studied anodic WO_3 films by Raman spectroscopy. These two groups observed that insertion of H^+ or Li^+ was accompanied by the appearance or increase of a band at about 950 cm^{-1}. This band was assigned to the stretching mode of terminal W=O bonds.

On the other hand, Ohtsuka *et al.* (*4*) have examined the Raman spectra of anodic tungsten oxide and Habib *et al.* (*5*) the infrared spectra of WO_3 films produced from WCl_6. These two latter groups claim that their results can be interpreted according to the reaction:

$$W^{6+}{=}O + xH^+ + xe^- \rightleftarrows W^{5+}{-}OH \text{ (colored)}. \quad (2)$$

Recently, Kitao *et al.* (*6*) observed a new band at 2400 cm^{-1} by proton coloration in the infrared reflection spectra of sputtered tungsten oxide films. They assign this new band, which increases in intensity with the amount of inserted charge, to the stretching mode of OH radicals incorporated into the WO_3 matrix.

Thus, one is faced with two kinds of contradictory conclusions. Before discussing mechanisms, it is obviously necessary to clarify the experimental facts. This is why we have undertaken a new infrared study of sputtered tungsten oxide films using well defined experimental conditions. Normal transmission, which is the more

* To whom correspondence should be addressed.

0022-4596/93 $5.00

direct and unambiguous technique, is mainly used. However, specular reflexion was also used for comparison with the literature results.

Experimental

Tungsten oxide films were produced by radiofrequency (rf) magnetron sputtering from a tungsten target in an argon/oxygen (10%) plasma (*7–9*). Identical deposition conditions were used for all the samples, but the substrates varied depending on the kind of infrared experiment to be performed. The thickness of the films was evaluated with a Tencor alpha-step 200 apparatus. Several measurements were performed on different films and at different places on a given film. They indicate an uncertainty of about ±100 Å for films of between 3000 and 4000 Å thickness.

For the transmission experiments, tungsten oxide films of 3800 Å thickness were deposited onto ITO/silicon substrates. ITO is an Indium Tin Oxide electrode produced by rf magnetron sputtering at low temperature (*10*). We selected the sputtering conditions to obtain a 500 Ω/cm^2 resistivity, which is a good compromise between infrared transparency and electronic conductivity for ITO to be used as current collector. The silicon substrate was a polished undoped silicon wafer of 0.5 mm thickness. Rectangular pieces 2 × 1 cm were cut from the wafer. ITO was deposited on the whole surface and tungsten oxide only on half the surface (1 cm^2) in such a way that each tungsten oxide layer was studied with its own background.

For the infrared reflection experiments, tungsten oxide films of 3500 Å thickness were sputtered onto an ITO/glass substrate with a highly conducting (5 Ω/cm^2) and hence reflecting ITO coating (*8, 9*). Let us note that these latter samples are those used in prototypes of smart windows described elsewhere (*9*). We have also used for comparison a 3000 Å WO_3 deposit on aluminium.

The Li^+ insertion was performed in a glove box under argon atmosphere (<2 ppm water and oxygen) using 1 *M* CF_3SO_3Li in propylene carbonate as electrolyte. The amount of water in the electrolyte, measured by the Karl–Fischer method, was less than 10 ppm. This was achieved by heating CF_3SO_3Li under vacuum at 423 K for 72 hr and distilling the solvent under 4-Å molecular sieves. Lithium metal was used as the reference and counterelectrode. The amount of Li^+ introduced in the layer was measured with a potentiostat PJT 24-1 coulometer IG6N Tacussel equipment. Conversely, the amount of extracted Li^+ was controlled during the bleaching operation. A chronocoulometric technique was used with cathodic and anodic potentials of respectively 2 and 3.9 V/Li.

Once a layer was colored or bleached, it was rinsed with dry methanol and mounted in a homemade vacuum chamber either in the transmission or in the reflection mode. This chamber can be introduced inside the glove box and evacuated by an internal line connected to a vacuum pump. During the infrared experiments the sample was always kept under vacuum.

In the case of H^+ insertion we used H_2SO_4 aqueous solutions as the electrolyte. The coloration or bleaching was performed in the surrounding atmosphere and the layer was quickly rinsed with distilled water and acetone before being mounted in the vacuum chamber. A saturated calomel electrode (SCE) was used as the reference and a platinum foil as the counterelectrode. The quantity of inserted/extracted charge was again controlled by a chronocoulometric technique.

For the 3500-Å WO_3 films deposited on highly conducting ITO, the applied potential was taken in the range −0.4 to +0.5 V/SCE. An example of correspondence between the applied potential and inserted/extracted charge is given in Fig. 1. At the more negative potentials, electrochemical side reactions and in particular hydrogen evolution occur as shown by the increasing

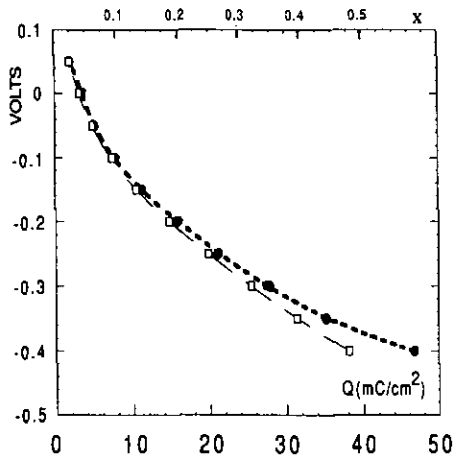

FIG. 1. Quantity of inserted (black circles, heavy dashed line) and extracted (open squares, light dashed line) protons in the potential range 0.05 to −0.4 V for a WO_3 (3500 Å)/ITO/glass sample dipped in a 1 *M* H_2SO_4 aqueous solution with a platinum counterelectrode and a calomel reference electrode. The amount of exchanged charge is measured at a given potential until the current becomes negligibly small; i.e., for about 10 min in coloration and for up to 30 min in bleaching operations performed under +0.3 V.

difference between the two curves. Nevertheless, about 40 mC · cm^{-2} are effectively extracted at −0.4 V. Using a density of 5.4 ± 0.1 g · cm^{-3}, one deduces the bronze composition $H_{0.5+0.01}WO_3$. This x value is higher than those previously given in the literature (*1*). Habib *et al.* (*11*) have recently shown that sputtered films of 800 Å thickness and 6.2 g · cm^{-2} density insert a maximum charge of 8 mC · cm^{-2} ($x = 0.4$). We have no explanation for the high x values we reach in the proton insertion process, but the important point for our spectroscopic experiments remains the possibility of comparing films at different coloration states, even if the absolute scale has to be shifted for some reason. The optical efficiency of these WO_3/ITO/glass samples at 633 nm has been found to take the rather normal value of 48 $cm^2 \cdot C^{-1}$ (*9*).

In the case of the 3800-Å films deposited on ITO/Si for the transmission experiments, the applied potential was taken in the range from −0.7 to +0.8 V/SCE to compensate for the voltage drop due to the high resistivity of ITO. Again a maximum x value of about 0.47 has been reached.

The infrared spectra were recorded with a Nicolet 740 FTIR spectrometer equipped with a cooled MCT (mercury cadmium telluride) detector and a KBr beam splitter. As the spectral range is then limited to 450 cm^{-1}, the 600–50 cm^{-1} region was also investigated in some cases with a 20F Nicolet FTIR spectrometer. However, this latter spectral range, which contains essentially the W–O deformation modes, proved to be only slightly sensitive to the coloration or bleaching and the results are presented mainly for the midinfrared range.

In a typical transmission experiment, the resolution was 4 cm^{-1} and 100 spectra were co-added. The background was recorded for the empty chamber equipped with two cesium iodide or polyethylene windows, then the reference for the ITO/Si substrate in the chamber was recorded, and finally the WO_3/ITO/Si sample. The reference was subtracted from the sample after both were ratioed to the background. As already pointed out (*2*), this standard procedure is not quite correct because of significant reflectivity changes between the reference and the sample. Consequently, some parts of the spectra appear with negative absorbances. However, we have not considered these effects in the present work and have focused our analysis on a comparison of the relative shapes and intensities of the absorption bands.

In the reflection mode at 12 or 56°, the sample was simply ratioed to a background given by a standard gold mirror.

The homemade chamber can be connected to a small reservoir containing heavy water. Thus, D_2O vapor pressure can be introduced inside the chamber in order to exchange *in situ* any O–H group with O–D. Three or four such operations yielded generally more than 90% isotopic exchange.

Results

1. Ageing of a Sputtered Tungsten Oxide Film

As in the preceding work (*2*), we have observed that the infrared spectrum of a layer evolves rather quickly as soon as it is taken out of the sputtering chamber and left in the surrounding atmosphere. An equilibrium is reached after a few months.

Acceptable electrochromic properties are observed for layers kept under vacuum and exposed to the atmosphere only during the transfer operations. We have chosen to study such layers by infrared spectroscopy because it would be very difficult to perform all the experiments just after sputtering.

Two typical transmission spectra of initial and aged films are presented in Fig. 2a. Tungsten oxide is characterized mainly by two broad absorption bands centered at about 700 and 300 cm^{-1}. They correspond, respectively, to the stretching and bending modes of the W–O framework in an amorphous material (*2*). The other absorptions come from species which involve labile hydrogen atoms, as shown by the H/D exchange represented in Fig. 3.

Figures 2b and 2c show that adsorbed water is initially present ($\nu_{OH_2} \sim 3400$ and $\delta_{OH_2} \sim 1620$ cm^{-1}), whereas new hydrogenated species are formed in the atmosphere. The latter are characterized mainly by strong absorption bands at 3178, 3034, and 1420 cm^{-1}. These frequencies are unusual for W–O–H groups; in hydrogen bronzes the WOH deformation mode has been identified at about 1170 cm^{-1} by inelastic neuton scattering (*12*). But rather than a process of proton insertion, we believe that ageing corresponds to hydrolysis of reactive surface sites by atmospheric water vapor. Bronsted acid centers are then formed on the surface. They are highly reactive and in particular their aptitude to protonate ammoniac to give ammonium ions is well known (*13*). The new absorptions which appear at 3178, 3034, and 1420 cm^{-1} are characteristic of NH_4^+ ions. According to the usual nomenclature (*14*), they correspond, respectively, to the ν_3, ν_1, and ν_4 vibrational modes of NH_4^+. Other weaker absorptions at 1675 cm^{-1} (ν_2), 2849 cm^{-1} ($2\nu_4$), 2062 cm^{-1} ($\nu_2 + \nu_6$), and 1810 cm^{-1} ($\nu_4 + \nu_6$) allow a more complete assignment of the adsorbed ammonium ions to be made (*14*).

A complementary experiment has been set up to confirm the strong affinity of sputtered tungsten oxide toward ammoniac. A WO_3/ITO/glass sample (with ITO 5Ω/cm^2 resistivity) has been exposed for 5 min to ammoniac gas. The IR spectra of the WO_3 layer before and after exposure have been recorded in the reflection mode at 58°. Actually, these spectra (Fig. 4) correspond to double absorption in the WO_3 layer and they greatly favor the higher frequency part, as expected from IRRAS (infrared reflection absorption spectroscopy).

In the difference spectra of Fig. 4c, the NH_4^+ absorptions show up very clearly, confirming definitely the previous assignment.

It must be pointed out that an aged layer submitted to progressive heating loses first the adsorbed water molecules at about 500 K, then the NH_4^+ adsorbed ions at above 600 K, just before crystallization into the stable monoclinic form.

2. Coloration/Bleaching Process

Spectra taken in the transmission mode are presented in Fig. 5 for sputtered tungsten oxide films, colored either by proton or lithium injection, after subtraction of the ITO/Si substrate.

The more striking effect is the strong absorption increase toward the near-infrared with increasing x values. Actually, this is the wing of the well known absorption band centered at about 1.4 eV in the visible region (*1, 7*). An expanded view is also presented in the region of the vibration ν_{W-O} (Fig. 6).

The variation of the water and hydroxyl content during the coloration/bleaching cycles is the same as previously reported (*2*): Upon H^+ insertion, the water quantity in-

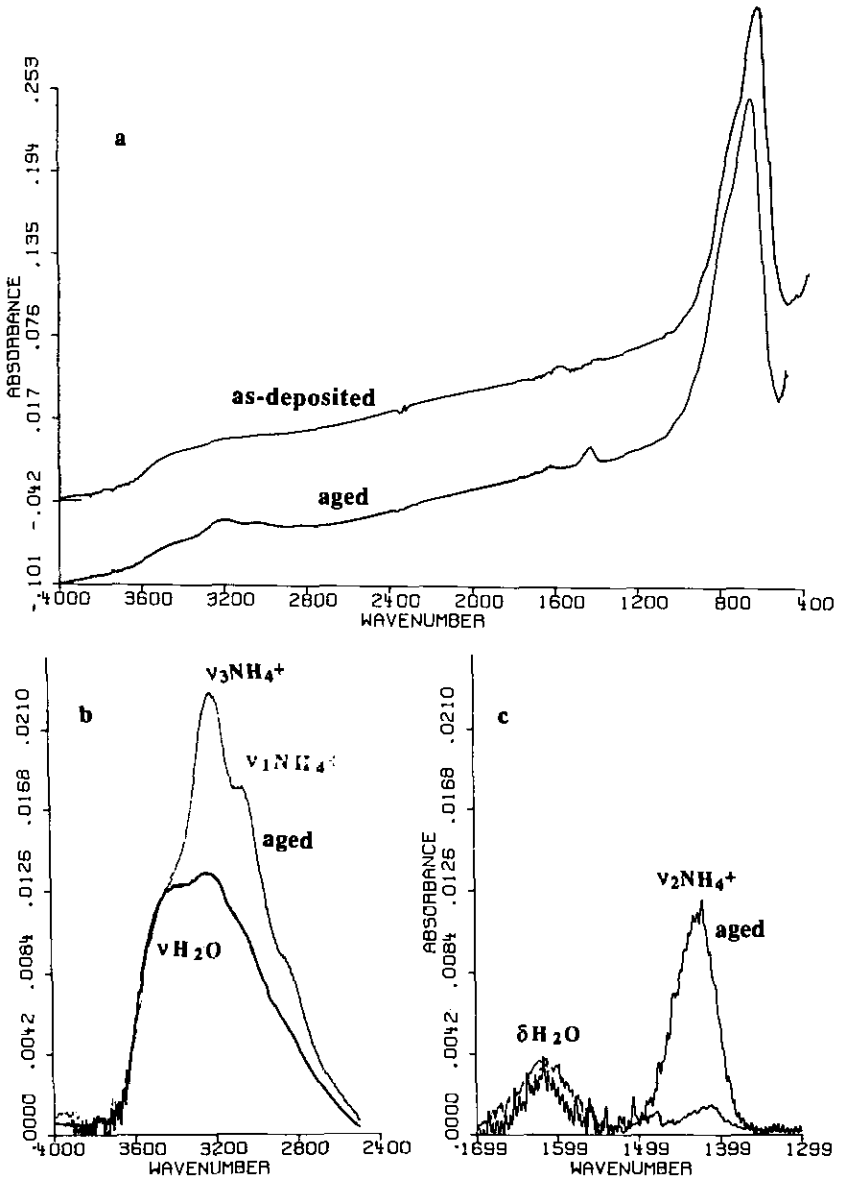

FIG. 2. Infrared spectra of 3800-Å tungsten oxide layers on silicon: (a) just after sputtering (upper spectrum) and after several months (lower spectrum). Spectra (b) and (c) are expanded views of the OH stretching and bending regions, respectively, after base-line correction.

creases very much at the first coloration and then oscillates about an equilibrium value which is always slightly smaller in the bleached state than in the colored one. At the same time, the NH_4^+ adsorbed ions disappear continuously and become negligible after ten cycles.

Upon Li^+ coloration, the water content does not increase noticeably. The 1420 cm^{-1} $\nu_{4(NH_4^+)}$ band disappears on cycling but at a much smaller rate than with H^+. Bleaching produces always the same kind of spectrum in which the amount of water is strongly reduced by cycling.

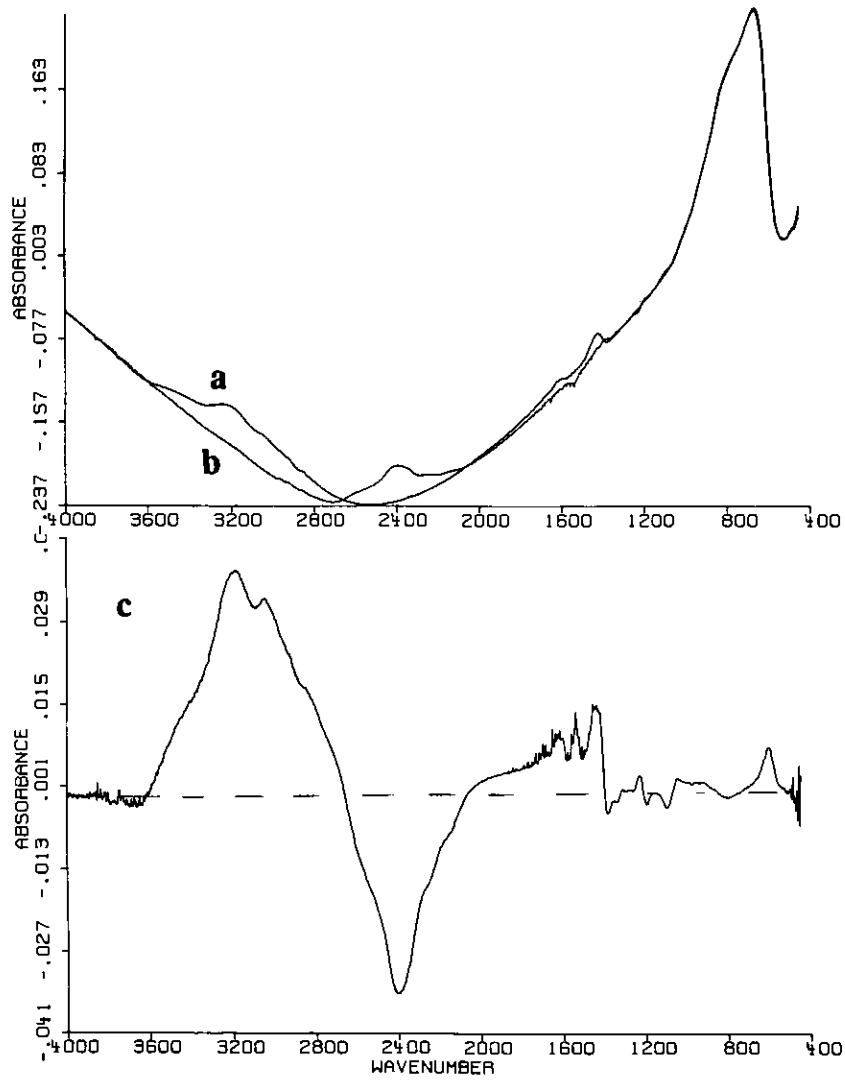

FIG. 3. Comparison of the infrared spectra of 3800-Å tungsten oxide films on ITO/Si before (a) and after (b) deuteration. Spectrum (c) corresponds to the difference between (a) and (b).

As already pointed out, the ν_{W-O} absorption profile is characterized by the appearance of a band or shoulder at 950–960 cm^{-1} under H^+ or Li^+ coloration. This band disappears reversibly on bleaching. We previously assigned this effect to the formation of terminal W=O bonds. The higher precision of the present spectra and the control of x allow a more careful analysis to be performed; in particular, we have presented in Fig. 7 the whole modification of the ν_{W-O} profile deduced from a subtraction of the spectrum of the bleached state from the spectrum of a given colored state. The 950–960 cm^{-1} absorption is now much better defined and, in addition, a strong absorption appears at about 570–600 cm^{-1} and some weaker bands are observed in between.

From these spectra, it is possible to

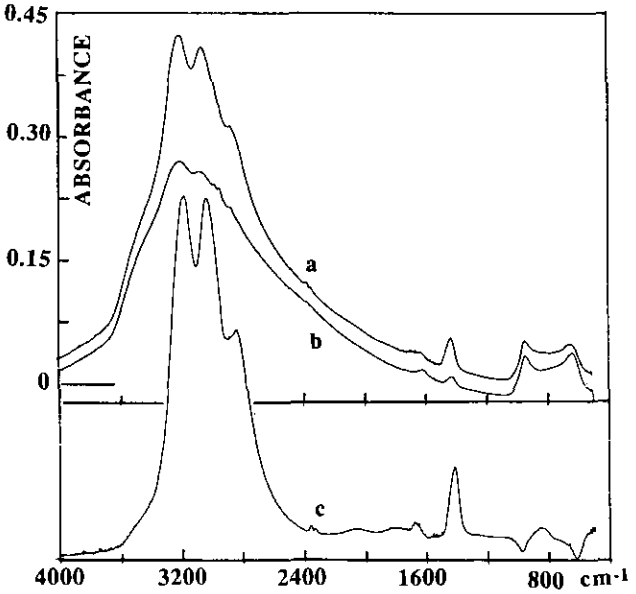

FIG. 4. Comparison of the infrared reflectance spectra at 58° of a 3500-Å tungsten oxide film on ITO/glass before (a) and after (b) 5-min exposure to ammoniac gas. The difference (b) − (a) is given in (c). The spectra are reported on an absorbance scale because they result mainly from double absorption in the film.

estimate both the intensity and the frequency of the different bands as a function of the nature of the inserted cation and of x (Fig. 8). These data confirm that the observed difference absorptions are associated to cation insertion. Indeed, there is a clear proportionality of the intensities with x. A surprisingly good agreement is even observed between the intensity evolutions for H^+ and Li^+ insertion (Figs. 8a and 8b). It can also be noted that the frequencies vary slightly, both with the nature of the cation and with the amount of inserted charge x. Proton insertion produces a stronger splitting of the two components (Figs. 8c and 8f) than lithium insertion (Figs. 8d and 8e). In both cases, the frequency of the maximum decreases when x increases.

Finally, WO_3 films sputtered on ITO/glass substrates have been analyzed in the reflection mode at 12° and 58°. As shown in Figs. 9 and 10, a huge reflectivity change occurs when H^+ or Li^+ ions are inserted in the films.

Discussion

1. Comparison with the Literature Results

The main question raised in the Introduction seems to definitely be clarified: insertion of protons or lithium in tungsten oxide layers induces a change of the νW–O profile with the previously observed appearance of an absorption band at 950–960 cm^{-1} (*2*) but also with a new intense feature at about 570–600 cm^{-1} and several other less well defined absorptions in between.

The experimental evidence for the inverse process, transformation of initial W=O bonds into W–OH groups by coloration, as reported recently (*4–6*), seems to be questionable.

Ohtsuka *et al.* claim that their *in situ* Raman spectra of anodic tungsten oxide (Fig. 9 of Ref. 4) resemble those of a precipitate

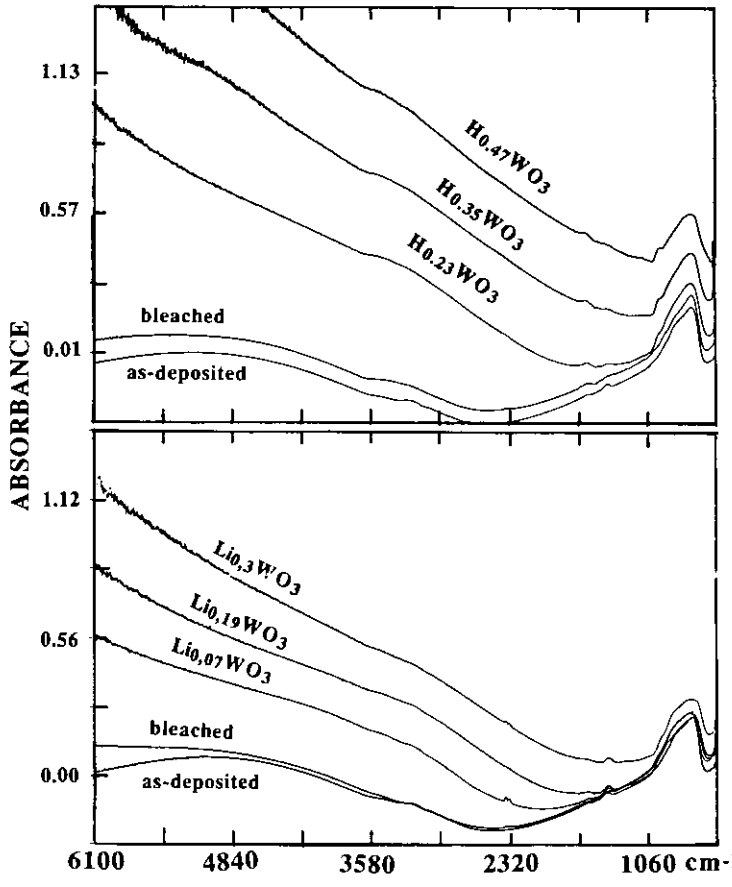

FIG. 5. Infrared transmission spectra of 3800-Å tungsten oxide layers on ITO/Si in different bleached and colored states. Top, H^+ insertion. Bottom, Li^+ insertion.

of tungstate solutions with hydrochloric acid and not at all the spectra of WO_3, $WO_3 \cdot H_2O$, or $Na_2WO_4 \cdot 2H_2O$. Actually, their spectrum of $WO_3 \cdot H_2O$ is not correct. The "true" spectrum presents a narrow line at 948 cm^{-1} and a broader one at 645 cm^{-1}, as reported in Ref. 16. In this latter paper the spectrum of $WO_3 \cdot 2H_2O$ is also given. It is characterized by a narrow line at 960 cm^{-1} and a doublet at 685–662 cm^{-1}. Therefore, the Raman spectrum of the anodic oxide film with lines at 960 and 670 cm^{-1} is very close to the spectrum of $WO_3 \cdot 2H_2O$, and hence W=O terminal bonds are effectively present in the starting material.

The evolution of this spectrum under proton insertion is analyzed by Ohtsuka *et al.* (*4*) in terms of a decrease of the intensity of the W=O line at 960 cm^{-1}. The data reported in their Figs. 8 and 9 indicate that cathodic reduction decreases the intensity of the whole spectrum to a stage where there is no more Raman signal at all. In this evolution, one can even remark that the 670 cm^{-1} band decreases faster than the 960 cm^{-1} one. We believe that the general intensity decrease illustrates the difficulty of recording a significant Raman signal for highly absorbing colored layers (*2, 3*).

The *in situ* infrared spectroscopic study of Habib *et al.* (*5*) is also rather puzzling. A band at 980 cm^{-1} assigned to W=O terminal bonds but not visible in their initial difference spectrum (Fig. 2) is supposed to "in-

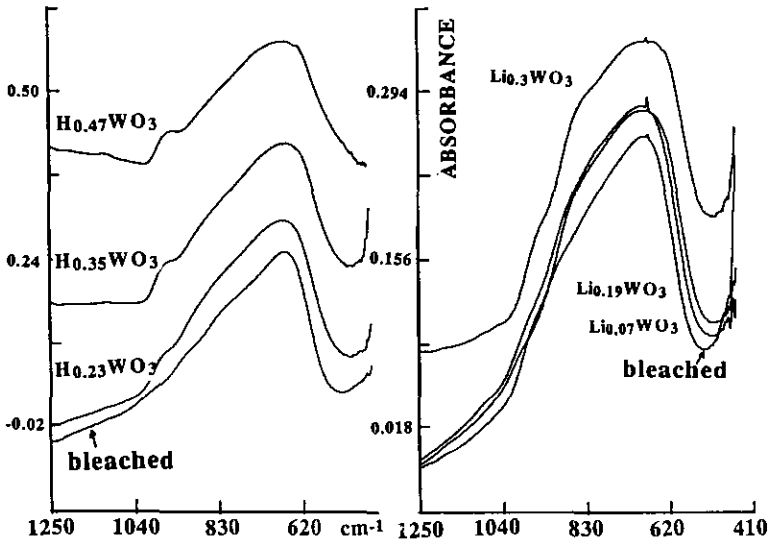

FIG. 6. Details of Fig. 5 in the ν_{W-O} region.

crease in the negative direction" when the applied cathodic potential increases. We believe that the precision of the experimental observation through the aqueous electrolyte layer is insufficient for a clear assignment in this spectral range.

Finally, the recent reflection results of Kitao *et al.* (*6*) can be compared to those re-

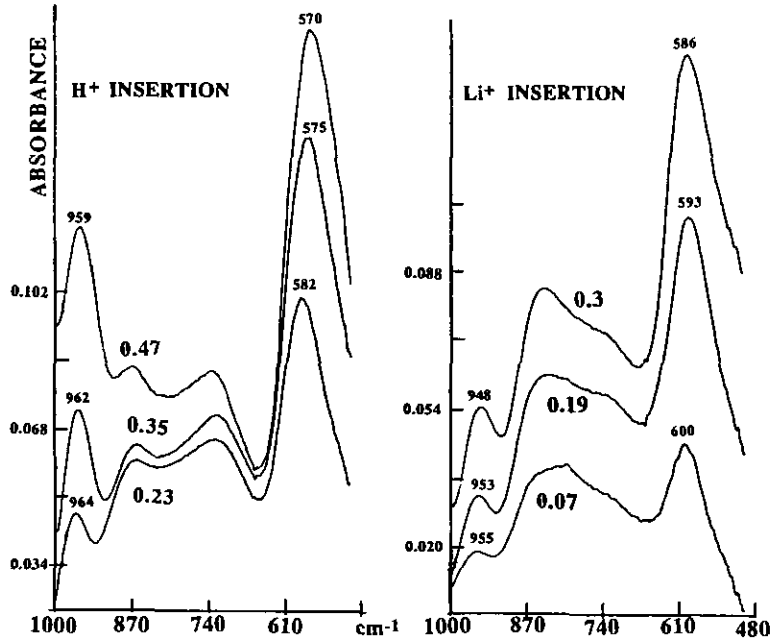

FIG. 7. Difference spectra (colored − bleached) in the ν_{W-O} region for H^+ insertion (left) and Li^+ insertion (right), with indication of the wavenumbers of the more characteristic absorptions.

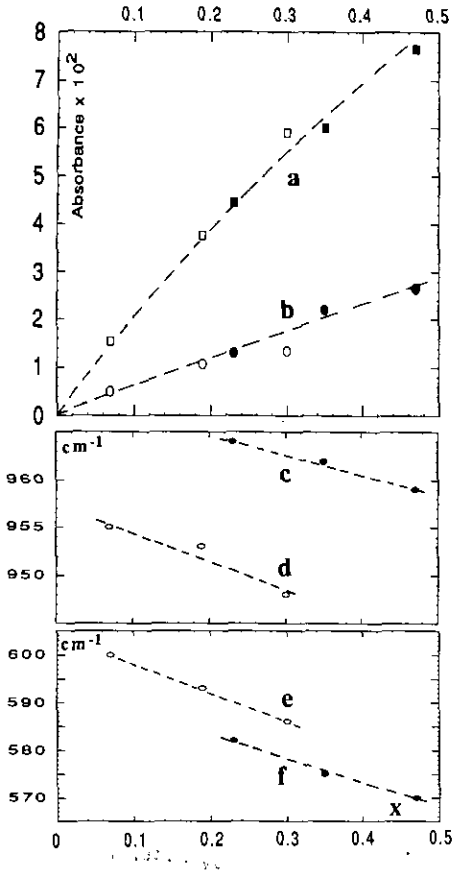

FIG. 8. Evolution of the high- and low-frequency components represented in Fig. 7, as a function of the amount of inserted charge x for H^+ insertion (black symbols) and Li^+ insertion (open symbols). The absorbance at the maximum of the bands at about 960 cm^{-1} (a) and 580 cm^{-1} (b) have been evaluated after a base-line correction. The position (cm^{-1}) of these two bands are reported for H^+ insertion (c) and (f) and for Li^+ insertion (d) and (e).

ported in Figs. 9 and 10. Those authors plot their data in an optical density scale as if the bleached and colored films were mainly absorbing the IR light. They assign the intense band at 2400–2000 cm^{-1} to hydroxyl group absorptions and claim that the intensity of this band is proportional to the amount of inserted protons.

Actually, our results rule out this assignment for several reasons:

—Li^+ insertion (Fig. 10) performed in a carefully dried electrolyte produces the same effect as H^+ insertion (Fig. 9).

—The new band undergoes a considerable frequency shift as a function of the amount of inserted Li^+ or H^+; at the highest insertion levels it is centered at about 1700 cm^{-1}.

—The intensity of this new band is not proportional to the amount of inserted charge; a maximum intensity (minimum reflectance) is reached for about 23 to 25 $mC \cdot cm^{-2}$ H^+. Then the intensity is decreasing (or the reflectance increasing).

—We have verified that the new band is insensitive to H/D exchange.

—Similar features are observed for WO_3 deposited on aluminum (Fig. 10), showing that the observed phenomena do not depend on the nature of the substrate.

2. Tentative Interpretation of the Present Data

We have confirmed our previous observations (*2*) but also added some new results which can help in the interpretation. Thus, coloration by H^+ or Li^+ cations is accompanied not only by the increase of a band at 950–960 cm^{-1} but also by the parallel growth of several other bands due to W–O stretching modes. To characterize the new W–O oscillators, it is tempting to use a correlation established between ν_{W-O} force constants (or wavenumbers) and W–O bond-lengths (*16*), although this approach is very qualitative since it implies more or less isolated W–O oscillators.

The initial tungsten oxide films can be considered to be formed of corner-sharing WO_6 octahedra with average W–O bond-lengths of about 1.8 to 1.9 Å (*17*). The disorder in these amorphous films is responsible for the broad and featureless absorption band centered at about 700 cm^{-1} (Fig. 6). The new bands of the colored state at 950 and 580 cm^{-1} would correspond, according to our correlation (Fig. 10 of Ref. 16), to

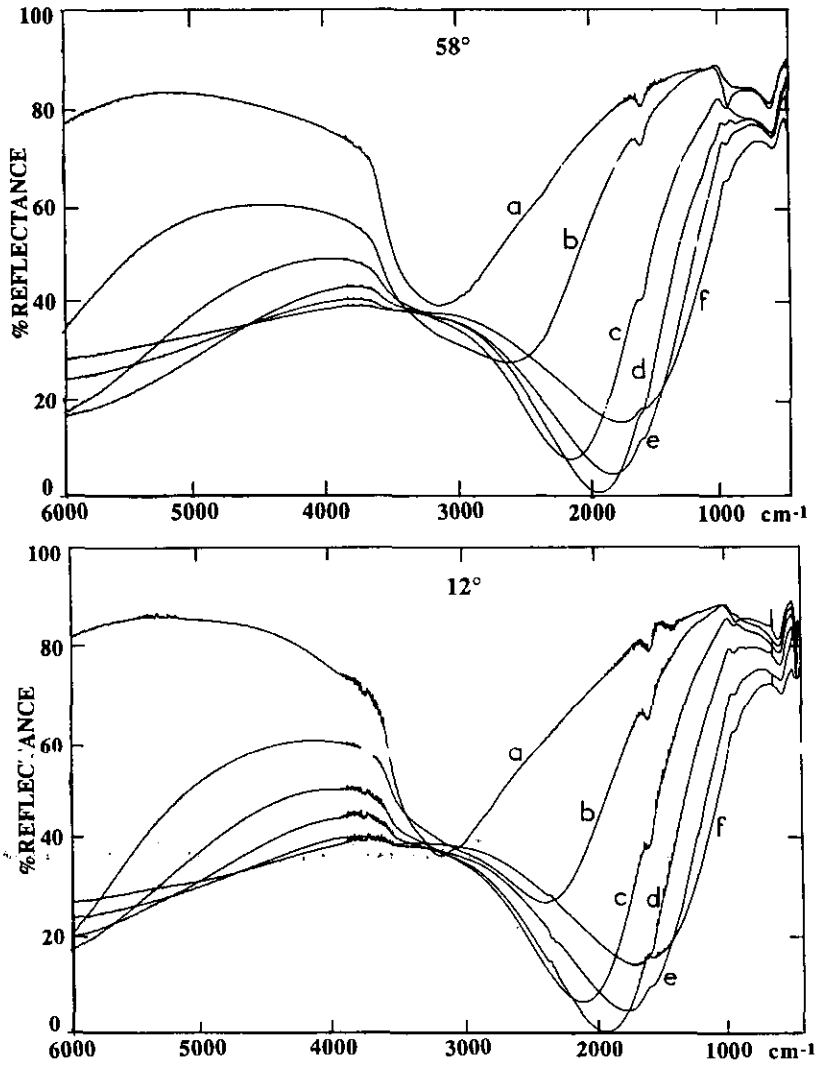

FIG. 9. Reflectance spectra of WO3 (3500 Å)/ITO/glass at various H^+ insertion levels. Top, 58°: (a) as-deposited film, (b) 10.7 mC · cm^{-2}, (c) 16.6 mC · cm^{-2}, (d) 23.2 mC · cm^{-2}, (e) 31.2 mC · cm^{-2}, (f) 397.5 mC · cm^{-2}. Bottom, 12°: (a) as-deposited film, (b) 12 mC · cm^{-2}, (c) 18.2 mC · cm^{-2}, (d) 24.8 mC · cm^{-2}, (e) 30 mC · cm^{-2}, (f) 39 mC · cm^{-2}.

W–O bond lengths of 1.7 and 2 Å, respectively.

Thus, one can conclude that an increasing proportion of shorter (1.7 Å) and longer (2 Å) bonds is created by H^+ or Li^+ insertion. This is quite in agreement with the concept of small polaron (*18*) in which coloration proceeds by electron trapping on a tungsten site to give a local lattice perturbation around the W^{5+} site. The H^+ or Li^+ compensating charge then arrives close to the distorted octahedron and interacts with a given oxygen atom as schematized in Fig. 11. Visible light absorption responsible for the blue coloration can then occur between the two adjacent tungsten atoms according to (*19*):

$$W_A^{5+} + W_B^{6+} \overset{h\nu}{\rightleftharpoons} W_B^{5+} + W_A^{6+}. \quad (6)$$

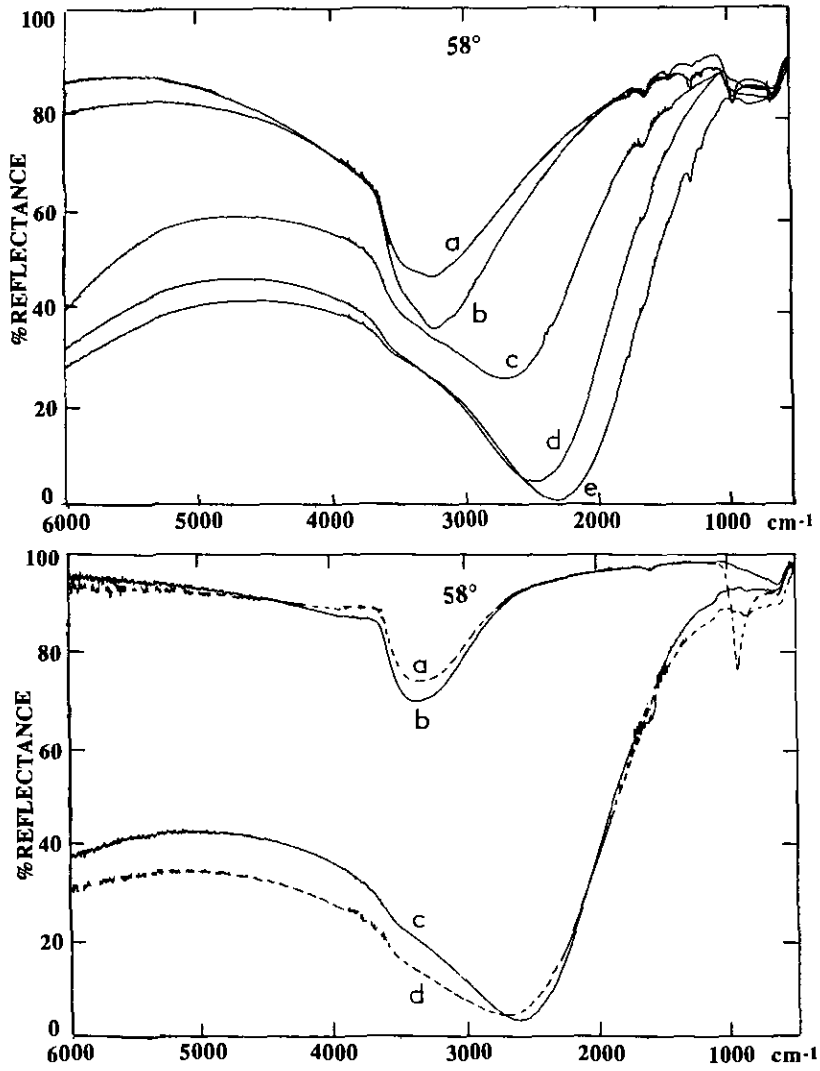

FIG. 10. Reflectance spectra at 58°. Top, WO3 (3500 Å)/ITO/glass for various Li^+ insertion levels: (a) bleached, (b) as-deposited, (c) 20 mC · cm^{-2}, (d) 30 mC · cm^{-2}, (e) 40 mC · cm^{-2}. Bottom, WO3 (3000 Å)/Al under *s* (solid lines) or *p* (dashed lines) polarization: (a) and (b), as-deposited; (c) and (d), about 30 mC · cm^{-2} H^+ insertion.

Of course, Fig. 11 is a very crude representation of the whole process for at least three main reasons: Only axial perturbations of the W–O bondlengths are considered, the role of the water molecules initially present in the layer is not taken into account, and the exact position of the inserted proton or lithium is not known.

Figure 7 indicates that absorptions of non-negligible intensity appear between the 960 and 580 cm^{-1} bands, especially in the case of Li^+ insertion. They can correspond to equatorial bonds perturbations or/and to perturbations at longer distances relative to the W^{5+} site.

We have seen that some water is present in the native WO_3 layers and a fortiori in the aged ones. It has been argued often in the

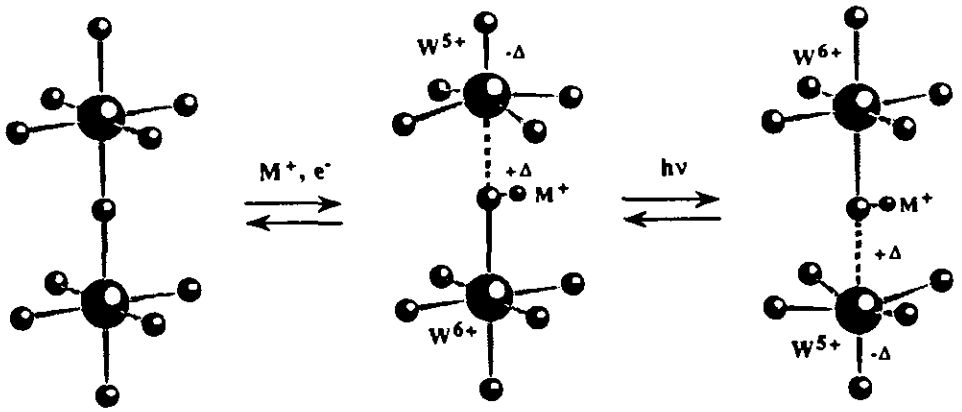

FIG. 11. Schematic representation of the lattice distortion occurring upon cation insertion in the tungsten oxide layer. The bleached state is represented on the left with W–O distances of about 1.8–1.9 Å. The colored state involves shorter and longer W–O bonds indicated by the symbols $-\Delta$ and $-\Delta$, respectively.

literature that these water molecules play an important role in insertion kinetics (*1, 20*). According to our previous (*2*) and present estimations, the proton insertion process (Eqs. (1) and (3)) could be written in the more realistic form

$$WO_{3-y}, mH_2O + xH^+(H_2O)_n + xe^- \rightleftarrows H_xW_x^{5+}W_{1-x}^{6+}O_{3-y}(H_2O)_{m+nx}, \quad (4)$$

where $y = 0.1$ to 0.2, $m = 0$ to 0.3 according to the ageing state, and $n = 0.7$. A similar equation has been proposed by Lusis *et al.* (*20*).

It has not been possible, up to now, to differentiate structural, adsorbed, and protonated water in the IR spectra.

Our data (Figs. 7 and 8) reveal differences between proton and lithium insertion, with stronger perturbations of the host lattice for the former. Structural determinations on the lithium bronze $Li_{0.36}WO_3$ indicate a distortion of the vacant perovskite-like cavities upon lithium insertion (*21*). These cavities are occupied by Li in square planar coordination with Li–O distances of about 2.2 Å. In our amorphous materials, this value is certainly an upper limit and an even shorter distance is expected for the proton–oxygen distance.

The reflection experiments reported in Figs. 9 and 10 confirm that cation insertion in the films produces the huge, previously reported (*6*), spectral changes in the midinfrared.

As already pointed out, the spectra of the as-deposited and bleached films certainly undergo a double absorption process since tungsten oxide is then a very poor conductor. The main band at 3400 cm^{-1} is easily assigned to the OH stretching modes of adsorbed water. It shifts to about 2500 cm^{-1} by H/D exchange, as already seen from the data of Fig. 3.

When cations are inserted, the material becomes semiconducting and even reaches a quasi-metallic state at high insertion levels (*1, 18, 19*). We have seen that the new band appearing between 2500 and 1700 cm^{-1} can by no means be assigned to hydroxyl groups. Neither can it be assigned to any other kind of absorption since an extremely large absorbance value would be reached at 1944 cm^{-1} for 24 mC/cm^2 H^+ insertion and at 2200 cm^{-1} for 40 mC/cm^2 Li^+ insertion (Figs. 9 and 10). When the ITO substrate is changed for aluminum (Fig. 10), the gross effect is conserved but the minimum reflectance is slightly shifted to higher wavenumbers and differences occur toward the

near-infrared. The latter are certainly caused by the decreasing ITO reflectivity in this frequency range.

Finally, the comparison of the reflectance spectra at 58° and 12° (Fig. 9) and of those obtained at 58° under p or s polarization (Fig. 10) rules out the hypothesis of an excitation having a longitudinal character such as a plasmon.

We have thus envisaged the possibility of interference effects of variable amplitude depending on the refractive index of the film. The interference pattern would be strongly perturbed at high wavenumbers by the intense absorption wing of the colored sample (Fig. 5) and at low wavenumbers by the WO_3 vibrational bands. This interpretation has been fully confirmed by thin-film optics calculations using a program developed in this laboratory (*22*). The known optical constants of ITO and thickness of WO_3 have been introduced and the optical constants of H_xWO_3 have been fitted. The spectra of Figs. 9 and 10 are perfectly simulated with quite reasonable values of the optical constants for the bronzes. The details of this calculation and of the results will be published in a forthcoming paper.

Conclusion

Our new infrared spectroscopic results on bleached and colored sputtered tungsten oxide films confirm the appearance of a band at 950–960 cm^{-1} upon H^+ or Li^+ insertion (*2, 3*) and rule out the hypothesis of formation of $W^{5+}OH$ groups from W=O bonds (*4, 5*) or of any kind of hydroxyl group (*6*).

The 960 cm^{-1} band was previously assigned to the stretching vibration of W=O terminal bonds. A more complete analysis of the infrared spectra indicates that it is part of a more general modification of the WO_6 octahedra vibrations. We assign the 960 cm^{-1} band to the stretching vibration of short W–O bonds (1.7 Å) close to a W^{5+} reduced site and a band at about 584 cm^{-1} to simultaneously lengthened W–O bonds (2 Å) linking the adjacent W^{6+} site (Fig. 11).

An interesting point would be to confirm now this small polaron picture by a Raman characterization of the intervalence charge transfer between adjacent W^{5+}/W^{6+} sites. This charge transfer is expected to be governed by some specific vibrational mode(s) of the M_xWO_3 lattice. By a judicious choice of the laser exciting wavelength relative to the visible absorption band, one can hope to observe Raman resonance effects for some specific vibration(s) (*23*).

Another important aspect is the influence of the nature of the starting material on the observed phenomena. Differences certainly exist between amorphous and crystalline tungsten oxides. We have already observed that the sputtered films annealed at 600 K give a spectrum very close to the one of the monoclinic stable form (*2*). Cation insertion in this annealed film leads to spectral modifications very different from those described above.

A further parameter is the amount of inserted charge x. In the case of Li^+ insertion, we have observed irreversible spectral changes in the ν_{W-O} profile for $x > 0.3$. A major structural rearrangement seems to occur. Furthermore, let us recall that in similar materials the electronic conductivity has been shown to increase by several orders of magnitude above this x value (*1*). This has been interpreted in terms of transition from a semiconducting to a metallic behavior. Actually, the IR reflection spectra seem to be extremely sensitive to these conduction properties but the interpretation of these spectra is not straightforward.

Thus, several new experimental observations still need more detailed analyses for a better understanding of the WO_3 electrochromic properties. The aim of the present work was just to clarify serious literature contradictions on the more elementary experimental observations and to show that complex optical effects occur in the midinfrared spectra of these electrochromic films, especially in the reflectance mode because of interference effects.

Acknowledgments

The authors are grateful to Drs. C. Sourisseau, B. Desbat, and T. Buffeteau for stimulating discussions.

References

1. W. C. Dautremont-Smith, *Displays* **4,** 3 (1982).
2. M. F. Daniel, B. Desbat, J-C. Lassègues, and R. Garié, *J. Solid State Chem.* **73,** 127 (1988).
3. P. Delichère, P. Falaras, M. Froment, and A. Hugot-Le-Goff, *Thin Solid Films* **161,** 35 (1988).
4. T. Ohtsuka, N. Goto, and N. Sato, *J. Electroanal. Chem.* **287,** 249 (1990).
5. M. A. Habib and S. P. Maheswari, *J. Electrochem. Soc.* **138,** 2029 (1991).
6. M. Kitao, S. Yamada, S. Yoshida, H. Akram, and K. Urabe, *Sol. Energy Mater.* **25,** 241 (1992).
7. H. Kaneko, F. Nagao, and K. Miyake, *J. Appl. Phys.* **63,** 510 (1988).
8. H. Arribart, C. Padoy, A. Dugast, M. Armand, F. Defendini, and B. Desbat, Europ. Patent No. 0253713 (1987).
9. J.-C. Lassègues and D. Rodriguez, *in* "Optical Materials Technology for Energy Efficiency and Solar Energy Conversion," EOS/SPIE Proceedings, 1992, in press (1993).
10. S-J. Wen, Thesis, University of Bordeaux I, 1992.
11. M. A. Habib and S. P. Maheswari, *Sol. Energy Mater. Sol. Cells* **25,** 195 (1992).
12. R. C. T. Slade, A. Ramanan, P. R. Hirst, and H. A. Pressman, *Mater. Res. Bull.* **23,** 793 (1988).
13. A. A. Davydov, *in* "Infrared Spectroscopy of Adsorbed Species on the Surface of Transition Metal Oxides" (C. H. Rochester, Ed.), Wiley, New York (1990).
14. K. Nakamoto, "Infrared and Raman Spectra of Inorganic and Coordination Compounds," Wiley, New York (1978).
15. S. J. Green and Z. Hussain, *J. Appl. Phys.* **69,** 7788 (1991).
16. M. F. Daniel, B. Desbat, J. C. Lassègues, B. Gerand, and M. Figlarz, *J. Solid State Chem.* **67,** 235 (1987).
17. B. O. Loopstra and H. M. Rietveld, *Acta Crystallogr. Sect. B* **25,** 1420 (1969).
18. O. F. Schirmer, V. Wittwer, G. Baur, and G. Brandt, *J. Electrochem. Soc.* **124,** 749 (1977).
19. B. W. Faughnan, R. S. Crandall, and P. M. Heyman, *RCA Rev.* **36,** 177 (1975).
20. A. R. Lusis, J. J. Kleperis, A. A. Brishka, and E. V. Pentyush, *Solid State Ionics* **13,** 319 (1984).
21. C. J. Cava, A. Santoro, D. W. Murphy, S. M. Zahurak, and R. S. Roth, *J. Solid State Chem.* **50,** 121 (1983).
22. T. Buffeteau and B. Desbat, *Appl. Spectrosc.* **43,** 1027 (1989).
23. R. G. Egdell and G. B. Jones, *J. Solid State Chem.* **81,** 137 (1989).